https://doi.org/10.5194/angeo-2019-122
Preprint. Discussion started: 26 August 2019

Annales Geophysicae Discussions

Equatorial Plasma Bubbles Developing Around Sunrise Observed by an All-Sky Imager and GNSS Network during the Storm Time

Kun Wu[1,2], Jiyao Xu[1,2], Xinan Yue[3,2], Chao Xiong[4], Wenbin Wang[6], Wei Yuan[1,2], Chi Wang[1,2], Yajun Zhu[5], Ji Luo[1,2]

[1]State Key Laboratory of Space Weather, National Space Science Center, Chinese Academy of Sciences, Beijing, China

[2]College of Earth and Planetary Sciences, University of Chinese Academy of Sciences, Beijing, China

[3]Key Laboratory of Earth and Planetary Physics, Institute of Geology and Geophysics, Chinese Academy of Sciences, Beijing, China

[4]GFZ German Research Centre for Geosciences, Telegrafenberg, 14473 Potsdam, Germany.

[5]Institute of Energy and Climate Research (IEK-7), Forschungszentrum Juelich GmbH, Juelich, Germany

[6]High Altitude Observatory, National Center for Atmospheric Research, Boulder, CO, USA

Correspondence to: jyxu@spaceweather.ac.cn

Keywords: Equatorial plasma bubble near sunrise, Spread-F, All-sky imager, GNSS network

https://doi.org/10.5194/angeo-2019-122
Preprint. Discussion started: 26 August 2019

Annales Geophysicae Discussions Open Access EGU

Abstract.

A large number of studies have shown that equatorial plasma bubbles (EPBs) occur mainly after sunset, and they usually drift eastward. However, in this paper, an unusual EPB event was simultaneously observed by an all-sky imager and the Global Navigation Satellite Systems (GNSS) network in southern China, during the recovery phase of geomagnetic storm happened on 6-8 November 2015. Observations from both techniques show that the EPBs appeared near dawn. Interestingly, the observational results show that the EPBs continued to develop after sunrise, and disappeared about one hour after sunrise. The development stage of EPBs lasted for at least about 3 hours. To our knowledge, this is the first time that the evolution of EPBs developing around sunrise was observed by an all-sky imager and the GNSS network. Our observation showed that the EPBs drifted westward, which was different from the usually eastward drifts of post-sunset EPBs. The simulation from TIE-GCM model suggest that the westward drift of EPBs should be related to the enhanced westward winds at storm time. Besides, break and recombination processes of EPBs were observed by the all-sky imager in the event. Associated with the development of EPBs, increasing in the ionospheric F region peak height was also observed near sunrise, and we suggest the enhance upward vertical plasma drift during geomagnetic storm plays a major role in triggering the EPBs near sunrise.

1. Introduction

After sunset, plasma density depletions, also called equatorial plasma bubbles (EPBs), sometime occur in the equatorial- and low-latitude ionosphere. A large number of studies have shown that EPBs generally start to develop shortly after sunset during geomagnetic quiet periods (e.g., Weber et al., 1980; Kelley et al., 1986; Xiong et al., 2010; Wu et al., 2018). It is generally believed that the Rayleigh-Taylor instability (RTI) is a plausible mechanism to trigger the EPBs (Kelley, 2009; Makela and Otsuka, 2012). The growth rate of RTI is influenced by a number of different factors, such as the zonal electric field, neutral wind and the background ionospheric/thermosphere, as well as

https://doi.org/10.5194/angeo-2019-122
Preprint. Discussion started: 26 August 2019

the strength of magnetic fields (Ott, 1978; Abdu, 2001; Burke et al, 2004). The pre-reversal enhancement (PRE) of the eastward electric field around sunset is a main reason for the development of EPBs (e.g., Fejer et al., 1999; Abdu, 2001; Kelley, 2009; Huang, 2018). Owning to the intensified eastward electric field, near magnetic equator the ionosphere is rapidly elevated to higher altitudes via $E\times B$ drifts, which is favorable for the growth of RTI at the bottomside of the ionosphere.

The EPBs are thought to extend along magnetic field lines, and can reach as high as magnetic latitudes of about ± 20° (Kelley, 2009; Lühr et al., 2014). Xiong et al. (2016, 2018) suggest that EPBs have a typical zonal size of about 50 km, by using Swarm in situ electron density measurements as well as ground-based airglow imager. Although the characteristics of EPBs have been widely studied, special events, especially those occurring during geomagnetic storms, are still one of the interesting issues to be fully addressed. Some of the results showed that geomagnetic storms can affect the development of EPBs (e.g., Abdu et al., 2003; Tulasi et al., 2008; Carter et al., 2016), and in some extreme cases, the EPBs can extend to middle latitudes during intense geomagnetic storms (e.g., Sahai et al., 2009; Patra et al., 2016; Katamzi-Joseph et al., 2017; Aa et al., 2018). Moreover, in the storm time, EPBs near sunrise were occasionally observed by some instruments such as radar and satellite. Fukao et al. (2003) used observations from the Equatorial Atmosphere Radar to report EPBs near sunrise over the Indonesian region during a geomagnetic storm and suggested that the EPBs were likely associated with the geomagnetic storm. Huang et al. (2013) reported the observations of long-lasting daytime EPBs with the Communications/Navigation Outage Forecasting System (C/NOFS) satellite during a geomagnetic storm in which the EPBs were persistent from the post-midnight sector through the afternoon sector. Zhou et al. (2016) used observations from multiple low Earth orbiting satellites, like the Swarm constellation, the Gravity Recovery and Climate Experiment (GRACE) satellite, and the C/NOFS satellite, to detect the EPBs around sunrise during the St Patrick's Day storm. They suggested that the geomagnetic storm induced changes in ionospheric dynamics should be the reason for triggering the EPBs. But until now, there

https://doi.org/10.5194/angeo-2019-122
Preprint. Discussion started: 26 August 2019

has been no research on the occurrence characters and evolution of EPBs around sunrise using optical remote sensing, which can provide different aspects of the EPBs near sunrise.

It is well known that the EPBs usually drift eastward as reported by many studies (e.g., Pimenta et al., 2001; Martinis et al., 2003; Park et al., 2007; Taylor et al., 2013; Wu et al., 2017). However, during storm periods westward drifting EPBs have been also observed (Abdu et al., 2003; Basu et al., 2010; Santos et al., 2016). Abdu et al. (2003) reported some cases of EPBs that showed eastward drifts after sunset and later reversed to westward. Basu et al. (2010) reported that the westward drifting EPBs reached maximum velocities of about 80 - 120 m/s. Santos et al. (2016) also showed some EPBs of zonal drifts reversal (eastward to westward) during a geomagnetic storm, in which they suggested the Hall electric field caused the reversal.

From six-year observations of airglow image located in the southern China, we found only one case of EPBs starting to appear near sunrise during the storm recovery phase on 08 November 2015. The EPBs appeared before sunrise, kept developing and vanished in about 1 hour after sunrise. Unlike the quiet-time eastward drifting EPBs, the EPBs drifted westward. In the rest, we provide a detailed analysis of this event. In section 2, we give a general description of the instruments. Observational results are showed in section 3. In section 4, we provide comparisons with previous studies as well as discussions. Finally, summary is given in section 5.

2. Instrumentation

2.1 All-sky imager

The airglow data used in this study are obtained from an all-sky imager, which is deployed at Qujing, China (Geographic: 25° N, 104° E; Geomagnetic: 15.1° N, 176° E). Its location is indicated by the red star in Figure 1, and the blue circle represents the field of view (FOV) of the all-sky imager at an altitude of 250 km. The all-sky imager consists of a CCD detector (1024 × 1024 pixel), an interference filter (630.0 nm), and a fish-eye lens (FOV of 180°). The integration time of the all-sky imager is 3 min.

https://doi.org/10.5194/angeo-2019-122
Preprint. Discussion started: 26 August 2019

2.2 The Network of Global Navigation Satellite System (GNSS)

The GNSS data used in this study are derived from the Crustal Movement Observation Network of China (CMONOC), which consists of ~260 ground GNSS receivers covering the mainland of China. The information of these GNSS receivers has been given in previous publications (e.g., Aa et al., 2015; Yang et al., 2016; Zheng et al., 2016). The total electron content (TEC) was processed using the similar method as that described by Ding et al. (2014). Specifically, for each arc, the relative phase TEC was filtered using a band-pass filter. We then calculated the TEC residual of each arc for each pierce point, which the height of each ionospheric pierce point was about 300 km. Therefore, the TEC residual could indicate the occurrence of plasma bubbles. An elevation cutoff angle of 30° is used to reduce the multi-paths effects.

2.3 Digisond

The digisonde ionograms are obtained from a digisonde located at Fuke, a low-latitude station in the southern China (Geographic: 19.5° N, 109.1° E; Geomagnetic: 9.5° N, 178.4° W), and marked with a green dot in Figure 1. The virtual heights of the *F* layer were manually scaled by using the SAO Explorer software.

3. Observations and Results

Figure 2 shows the 3-hour *Kp* index, the interplanetary magnetic field (IMF) *Bz*, *SYM-H*, AE, AU, AL and h' F at Fuke on 06-08 November 2015. To make the comparison easier with other observations, we converted the universal time to the local time (LT) at Qujing. A geomagnetic storm occurred during those days. In Figure 2(b), IMF *Bz* turned southward at ~11:40 LT on 07 November 2015, and reached to about -11 nT at ~16:00 LT. During the storm main phase, the *SYM-H* had a rapid reduction from -40 nT to -100 nT. Meanwhile, the *Kp* index reached a value of 6; the AE and AL also reached at ~1500 nT and ~- 1500 nT, respectively. After 04:00 LT on 08 November 2015, IMF *Bz* began to turn to north. In the storm recovery phase, the value of *SYM-H* was back to

https://doi.org/10.5194/angeo-2019-122
Preprint. Discussion started: 26 August 2019

-40 nT.

Figure 3 shows the time sequence of airglow images observed by the all-sky imager at Qujing from 05:15 to 06:21 LT on 8 November 2015. The time difference between successive images is 6 min. For each image, we removed the effects of compression and curving of the all-sky imager lens by an unwarping process (Garcia et al., 1997). All images have been mapped into a geographic range from 97° to 111° E in longitude and from 18° to 32° N in latitude. The height of the airglow layer is assumed to be at 250 km. The top of each image is to the north and the right to the east. Two EPBs, marked as "b1" and "b2", were observed by the all-sky imager during this period. They occurred during the geomagnetic storm recovery phase.

Around 05:21 LT, EPB "b1" appeared in the FOV of the all-sky imager. "b1" was still developing, as it extended northward and reached close to 25° N around 06:21 LT. At 05:39 LT, the other EPB "b2" started to appear in the FOV of the airglow imager. "b2" was also developing and expanded to about 20° N at 06:21 LT. The two observed EPBs possibly continued to develop after 06:21 LT, as no hints of stop can be seen in the last airglow image. However, there was no further image data after 06:21 LT because the all-sky imager had to be shut down after sunrise. We want to pointed out that the sunrise time at Qujing was around 06:15 LT at altitude of 250 km on that day. The far north part of "b1" reached about 24.5°N at 06:15 LT. After 6 min, the far north of "b1" extended to about 25°N (as marked by the black horizontal line). In other words, the observational result from the all-sky imager suggested that the EPBs kept developing after sunrise.

Some interesting features can also be seen from Figure 3. "b1" appeared at ~105° E and "b2" appeared at ~104° E at 05:39 LT. Based on the black vertical line at 106° E, we can clearly see that the two EPBs drifted from east to west. Besides, break and recombination processes of EPB "b1" were also observed. After 05:45 LT, a break process occurred in "b1". The lower latitude portion of "b1" moved further to the westward. An obvious cleft occurred at ~19° N of "b1" near 06:03 LT. More interesting is the fact that a recombination process occurred in the two break portions of "b1"

https://doi.org/10.5194/angeo-2019-122
Preprint. Discussion started: 26 August 2019

during its later development period. After ~06:03 LT, the upper portion of "b1" began to connect to the lower portion of "b1" and they merged/combined together into one EPB after 06:15 LT. The break and recombination processes are more obvious in the red rectangles of Figure 3, which is indicated by the red arrow in each image.

Figure 4 shows a series of TEC residuals over 10°-50°N and 80°-130°E during 04:30-08:20 LT on 08 November 2015. The adjacent imaging is in 10 min intervals. At about 04:40 LT, some TEC depletions, which occurred to the south and west of the location of all-sky imager, appeared at ~115°E (~24°N), and began to develop. About 05:30 LT, some additional EPBs appeared at ~105°E (~20°N), and they were also developing. EPBs in the two regions kept developing until they disappeared. Owning to the FOV of the all-sky imager, the EPBs outside the ~115°E region were not observed.

In order to provide much more detailed comparison between the all-sky imager and TEC measurements, we chose those TEC variations of corresponding geographical area and time of each airglow imaging of Figure 3 in Figure 5. In Figure 5, the TEC variations show that the EPBs at ~105° E appeared near 05:30 LT, which correspond to EPB "b1" and "b2" observed by the all-sky imager. In Figure 5, TEC depletions move away from the 106° E with time (The black vertical line represents the 106°E in Figure 5), which is consistent with the movement of EPBs observed by the airglow imager. Meanwhile, the northernmost part of the depletion of ~105°E expanded to ~25°N at 06:20 LT (The black horizontal line represents the 25°N in Figure 5), which also agreed well with the observations of the all-sky imager. Interestingly, TEC variations show that the northernmost of EPBs of ~105°E extended beyond 25°N after 06:20 LT. We can see that the northernmost of them reached about 28°N at 07:10 LT in Figure 4. In other words, TEC variations show that the depletions of ~105°E were still there after 06:21 LT, and kept developing after sunrise, but vanished after ~08:00 LT. These observational results shown that the life time of those EPBs exceeds 3 hours.

4. Discussion

In this study we showed an special event of EPBs which was simultaneously observed by the all-sky imager and the ground GNSS network in the south China. One interesting

https://doi.org/10.5194/angeo-2019-122
Preprint. Discussion started: 26 August 2019

feature is that the EPBs started to appear near sunrise hours. Afterward, they kept developing until they totally vanished. During their life time, the EPBs moved from east to west. Those EPBs occurred in the recovery phase of the geomagnetic storm, which indicates that the prompt penetration electric fields (PPEF) and disturbance dynamo (DDEF), as well as disturbed neutral wind circulation may play an import role in triggering the EPBs.

The drift velocities of EPBs were shown in Figure 6. We used the cross sections (keogram) (Figures 6 (a), (c), and (e)) of the airglow images to separately calculate meridian velocities (Figure 6(b)) of "b1" and zonal velocities of "b1" at ~ 22°N (Figure 6(d)) and ~19°N (Figure 6(f)) geographical latitudes. Figure 6(a) illustrates the N-S cross sections (between 104°E and 105°E) of the airglow images shown in Figure 3. Figure 6(c) illustrates the W-E cross sections (between 21.5°N and 22°N) of the airglow images, and Figure 6(e) illustrates the W-E cross sections (between 18.5°N and 19°N). We separately calculated poleward and zonal velocities of "b1" based on the position of it changed over time in Figure 6(a), Figure 6(c) and Figure 6(e). The initial poleward and zonal velocities of "b1" were about 200 m/s and 60 m/s, respectively. Horizontal drift of EPB is also an important issue, which is often related to the background zonal plasma drift (Fejer et al., 2005; Eccles, 1998). The westward motion of the F-region should be caused by the ionospheric dynamo process in the early morning (Kil et al., 2000; Sheehan and Valladares, 2004). The drift direction of background zonal plasma drift has a reversal (eastward to westward) near dawn (Fejer et al., 2005). In our case, all EPBs emerged after 05:00 LT. The background plasma should drift westward during the early morning hours. So, it could partly explain why the observed EPBs drifted westward. In addition, the disturbed westward neutral winds can also contribute to the westward drifting of EPBs. Xiong et al. (2015) found that the disturbance winds were mainly towards westward at low latitudes, most prominent during early morning hours. Abdu et al. (2003) found that the westward drift of an EPB was most likely caused by westward zonal winds during a geomagnetic storm. Makela et al. (2006) found that the eastern wall of EPBs can become unstable due to the westward and equatorward neutral

https://doi.org/10.5194/angeo-2019-122
Preprint. Discussion started: 26 August 2019

winds associate with wind surges. In Figure 3, a sub-branch of dark bands first occurred at the eastern wall of "b1", indicated secondary instabilities developed at the eastern edge, most likely due to the westward disturbance winds.

In Figure 7, we used the Thermosphere-Ionosphere-Electrodynamics General Circulation Model (TIE-GCM) to simulate the horizontal winds on 08 November 2015 under magnetically active conditions, and the latitude versus longitude distribution of zonal wind velocities are shown at different times. The winds at 250 km are shown, and the spatial coverage has been confined to 0° - 40° N latitude and 90° - 120° E longitude. The dashed rectangles represent the location of "b1" and "b2" at different times. In Figure 7, we can see that the horizontal winds at low latitudes are mainly westward, which is consistent with the motion of EPBs in this case. As already discussed above, the westward drift of those EPBs is possibly caused by the westward disturbance winds. Besides, the zonal winds computed from TIE-GCM shown in Figure 7 are smaller than the zonal drifts of EPBs shown in Figure 6. This is because zonal drift value of EPBs was controlled by background zonal winds and ionospheric electric field (Haerendel et al., 1992; Eccles, 1998). The value differences between simulation and zonal drifts of EPBs should be influenced by ionospheric electric field.

As reported, most of the EPBs start to occur at pre-midnight hours. There were a very limited number of studies that used data from radar or satellite to report the occurrence of EPB close to sunrise hours (e.g., Fukao et al., 2003; Huang et al., 2013; Zhou et al., 2016). However, until now, there has been no observation result of EPBs around sunrise using optical remote sensing. In fact, it is very difficult to observe EPB near sunrise by an all-sky imager. Often, EPBs start to develop shortly after sunset and vanish before sunrise. Even though some EPBs occur around sunrise in their initial stage, they disappear when they drift eastward into the daytime. And almost no report shows that the EPBs still kept developing after sunrise. In our case, the developing EPB was first observed at about 05:30 LT (near dawn) by both the all-sky imager and the GNSS network. Our observational results show that they kept developing after sunrise, and vanished about one hour after sunrise. Those EPBs should be occurred near sunrise,

https://doi.org/10.5194/angeo-2019-122
Preprint. Discussion started: 26 August 2019

which is different from post-sunset EPBs. Their development stages lasted for at least about 3 hours.

In the rest, we try to explain why the EPBs occurred near sunrise. During the storm time, disturbance winds can affect the low-latitude ionospheric electrodynamics as well as the zonal drift of an EPB. The DDEF will drive plasma drift to move upward at nighttime during the development phase of storm (Blanc and Richmond, 1980). Meanwhile, a number of studies found the that high latitude electric fields can penetrate into the middle and low-latitude ionosphere as PPEF when IMF *Bz* turns southward or northward (Kelley et al., 1979; Scherliess and Fejer, 1997; Cherniak and Zakharenkova, 2016; Carter et al., 2016; Patra et al., 2016; Katamzi-Joseph et al, 2017). For the storm event, after IMF *Bz* turned southward at ~12:00 LT 07 November 2015, there was long duration and high AE in storm time. A DDEF should be present at recovery phase of storm time. And it reversed ambient electric field from westward to eastward near sunrise, which enhanced height of bottomside of the ionosphere *F*-region. Meanwhile, the northward turning of IMF *Bz* at ~04:00 LT 08 November 2015 caused over-shielding electric field, which produced an eastward PPEF into the low-middle latitude ionosphere. The eastward electric field also moved the *F* region ionosphere to higher altitudes via vertical $E \times B$ drifts. In Figure 2(e), the increased height of bottomside of the ionosphere *F*-region can be seen at Fuke. In low latitude region, one of the necessary conditions for the generation of EPBs is that the *F* layer should be uplifted to a higher altitude, where the RTI becomes unstable and forms EPBs. The *F* layer height is largely determined by the eastward field via the vertical $E \times B$ drift (Dabas et al., 2003).

In this study, EPBs were initially observed by the all-sky imager at about 05:15 LT. We think that only a portion of the EPBs were observed in our study, as EPB usually extend along the whole magnetic flux-tube. It also means that the EPBs should possibly occur before 05:15 LT at equatorial latitude. But due to the lack of observations at equator, we cannot provide direct evidence about their generation. However, as shown in our Figure 8, we also found that spread *F* began to appear in the ionograms from the digisonde at Fuke after 05:15 LT, which indicates that those EPBs occurred in the region

https://doi.org/10.5194/angeo-2019-122
Preprint. Discussion started: 26 August 2019

of southeastern Qujing (Note that Fuke is to the southeast of Qujing). Bottomside of the ionospheric F-region at Fuke was rapidly elevated from ~250 km to ~290 km near sunrise on 08 November 2015. The rapidly elevated height of the ionosphere can cause stronger RTI at the bottom of the ionosphere F-region, which is beneficial to the formation of EPB. The initial occurring time of EPBs of this case should be during this time. Unfortunately, we do not have more observations in the southeast of Fuke. We used the TIE-GCM to simulate the height of hmF2 at lower latitude on 08 November 2015. Figure 9 shows the hmF2 as a function of longitude and latitude at different times. The model results plotted are in a geographic range from 0° to 40° N in latitude and from 90° to 120° E in longitude. In Figure 9, we can see that hmF2 southeast of (the dashed rectangles) Qujing was rapidly elevated to higher altitudes near sunrise. In other words, when the IMF *Bz* turned northward at about 04:00 LT, the ionosphere in some regions southeast of Qujing could be rapidly elevated to higher altitudes at this time. Those EPBs occurred in the same time period as highlighted by the green rectangular area in Figure 2. Previous studies have reported that the occurrence of the dawn enhancement in the equatorial ionospheric vertical plasma drift (Zhang et al., 2015, 2016). They found that the enhancement of the ionospheric vertical plasma drift occurs around dawn. They suggested that the vertical plasma drifts can be enhanced near sunrise in a way similar to the PRE near sunset. Fejer et al. (2008) found that the nighttime disturbance dynamo drifts are upward, and have the largest values near rise. In our case, the model simulations and observations both show an increasing of the height of the ionosphere around sunrise. The enhancement of low-latitude ionospheric vertical plasma drift caused by DDEF and PPEF associated with the geomagnetic storm should play a vital role in triggering those EPBs. Our results also provide evidence of the enhancement of low-latitude ionospheric vertical plasma drift around sunrise, which should be the main reason of the EPBs generation near dawn.

In addition, some interesting features of EPBs are also shown in Figure 3 in that the EPBs showed also break and recombination processes. In Figure 6(f), at latitude of 19°N, the zonal velocity of “b1” was about 60-70 m/s between 05:20 LT and 06:15 LT.

https://doi.org/10.5194/angeo-2019-122
Preprint. Discussion started: 26 August 2019

Annales Geophysicae Discussions

However, at the latitude of 22°N (Figure 6(d)), the zonal velocity of "b1" was decreased from about 70 m/s to about 50 m/s between 05:20 LT and 05:45 LT. After 05:45 LT, its velocity began to increase from ~50 m/s to ~70 m/s from 05:45 LT to 06:00 LT. Then, it kept a velocity of ~70 m/s. Owning to the fact that the zonal velocity at higher latitudes was smaller than that at low latitudes before 05:45 LT, "b1" had a break process of EPBs during this period. After 05:45 LT, the zonal velocity at higher latitude was bigger than that at lower latitude, "b1" exhibited a recombination process of EPBs after 06:03 LT. The above results indicate that the break and recombination processes of EPBs should be caused by the different drift velocities of the background plasma at different latitudes.

5. Summary

In this paper, a special EPB event was observed by an all-sky imager and the GNSS network in the southern China. The evolution processes and characteristics of those EPBs were studied in detail. Our main findings are summarized as below:

(1) The observed EPBs on 08 November 2015 emerged before sunrise and kept developing. They dissipated at about one hour after sunrise (~ after 08:00 LT) and the development stage lasted for at least about 3 hours. The evolution of EPBs developing around sunrise was observed for the first time by an all-sky imager and the GNSS network.

(2) They occurred in the recovery phase of a geomagnetic storm. The enhancement of background ionospheric vertical plasma drift was also observed near sunrise. The rapid uplift of the ionospheric caused by the geomagnetic storm should be the main reason for triggering the EPBs.

(3) During the development, the EPBs drifted westward rather than eastward, The TIE-GCM simulation suggested that the westward drift of EPB is related to the westward disturbance winds.

(4) The EPB exhibited also break and recombination processes during its development.

https://doi.org/10.5194/angeo-2019-122
Preprint. Discussion started: 26 August 2019

Annales Geophysicae Discussions
Open Access
EGU

Acknowledgement

This work was supported by the Open Research Project of Large Research Infrastructures of CAS – "Study on the interaction between low/mid-latitude atmosphere and ionosphere based on the Chinese Meridian Project" and the Chinese Meridian Project, and the National Natural Science Foundation of China (41674152 and 41331069). The airglow and digisonde data were downloaded from http://data.meridianproject.ac.cn/. The airglow data used in this study can be obtained by contacting the corresponding author. We acknowledge the use of GNSS data from the Crustal Movement Observation Network of China (CMONOC, http:// neiscn.org/) and the data could be obtained upon request. We thank H. Liu from Macao University of Science and Technology for processing the GNSS data. The IMF, AE, AL, AU, KP, and SYM/H data are obtained from the CDAWeb (https://cdaweb.sci.gsfc.nasa.gov/) and the WDC for geomagnetism at Kyoto University (https://wdc.kugi.kyoto-u.ac.jp/). The National Center for Atmospheric Research is sponsored by the National Science Foundation.

https://doi.org/10.5194/angeo-2019-122
Preprint. Discussion started: 26 August 2019

References

Aa, E., Huang, W., Yu, S., Liu, S., Shi, L., Gong, J., Chen, Y and Shen, H.: A regional ionospheric tec mapping technique over china and adjacent areas on the basis of data assimilation, J. Geophys. Res., 120, 5049-5061, https://doi.org/10.1002/2015JA021140, 2015.

Aa, E., Huang, W., Liu, S., Ridley, A., Zou, S., Shi, L., Chen, Y., Shen, H., Yuan, T., Li, J., and Wang, T.: Midlatitude plasma bubbles over China and adjacent areas during a magnetic storm on 8 September 2017, Space Weather., 16, 321–331, https://doi.org/10.1002/2017SW001776, 2018.

Abdu, M. A.: Outstanding problems in the equatorial ionosphere–thermosphere electrodynamics relevant to spread f, J. Atmos. Sol. Terr. Phys., 63, 869-884, https://doi.org/10.1016/S1364-6826(00)00201-7, 2001.

Abdu, M. A.: Magnetospheric disturbance induced equatorial plasma bubble development and dynamics: A case study in Brazilian sector, J. Geophys. Res., 108, A12, https://doi.org/10.1029/2002ja009721, 2003.

Basu, S., Basu, S., MacKenzie, E., Bridgwood, C., Valladares, C. E., Groves, K. M., and Carrano, C.: Specification of the occurrence of equatorial ionospheric scintillations during the main phase of large magnetic storms within solar cycle, Radio Science., 45, RS5009, https://doi.org/10.1029/2009RS004343, 2010.

Blanc, M., and Richmond, A. D.: The ionospheric disturbance dynamo, J. Geophys. Res., 85, A4, https://doi.org/10.1029/JA085iA04p01669, 1980.

Burke, W. J., Gentile, L. C., Huang, C. Y., Valladares, C. E., and Su, S. Y.: Longitudinal variability of equatorial plasma bubbles observed by dmsp and rocsat-1, J. Geophys. Res., 109, 17, https://doi.org/10.1029/2004JA010583, 2004.

Carter, B. A., Yizengaw, E., Pradipta, R., Retterer, J. M., Groves, K., Valladares, C., Caton, R., Bridgwood, C., Norman, R., and Zhang, K.: Global equatorial plasma bubble occurrence during the 2015 St. Patrick's day storm, J. Geophys. Res., 121, 894-905, https://doi.org/10.1002/2015JA022194, 2016.

Cherniak, I., and Zakharenkova, I.: First observations of super plasma bubbles in

https://doi.org/10.5194/angeo-2019-122
Preprint. Discussion started: 26 August 2019

Europe, Geophys. Res. Lett., 43, 137–11,145, https://doi.org/10.1002/2016GL071421, 2016.

Dabas, R. S., Singh, L., Lakshmi, D. R., Subramanyam, P. , Chopra, P. , and Garg, S. C.: Evolution and dynamics of equatorial plasma bubbles: relationships to exb drift, postsunset total electron content enhancements and equatorial electrojet strength, Radio Science., 38, 1075, https://doi.org/10.1029/2001RS002586, 2003.

Ding, F., Wan, W., Mao, T., Wang, M., Ning, B., Zhao, B., and Xiong, B.: Ionospheric response to the shock and acoustic waves excited by the launch of the Shenzhou 10 spacecraft, Geophys. Res. Lett., 41, 3351–3358, https://doi.org/10.1002/2014GL060107, 2004.

Eccles., V. J.: A simple model of low-latitude electric fields, J. Geophys. Res., 103, 26699-26708, https://doi.org/10.1029/98JA02657, 1998.

Fukao, S., Ozawa, Y., Yamamoto, M., and Tsunoda, R. T.: Altitude extended equatorial spread F observed near sunrise terminator over Indonesia, Geophys. Res, Lett., 30, 2137, https://doi.org/10.1029/2003GL018383, 2003.

Fejer, B. G., and Scherliess, L.: Mid- and low-latitude prompt-penetration ionospheric zonal plasma drifts, Geophys. Res. Lett., 25, 3071–3074, https://doi.org/10.1029/98GL02325, 1998.

Fejer, B. G., Scherliess, L., and Paula, E. R. D.: Effects of the vertical plasma drift velocity on the generation and evolution of equatorial spread-f, J. Geophys. Res., 104, 859-869, https://doi.org/10.1029/1999JA900271, 1999.

Fejer, B. G., Souza, J. R., Santos, A. S., and Pereira, A. E. C.: Climatology of F, region zonal plasma drifts over Jicamarca, J. Geophys. Res., 110, A12310, https://doi.org/10.1029/2005JA011324, 2005.

Fejer, B. G., Jensen, J. W., and Su, S.-Y.: Seasonal and longitudinal dependence of equatorial disturbance vertical plasma drifts, Geophys. Res. Lett., 35, 20, https://doi.org/10.1029/2008gl035584, 2008.

Garcia, F. J., Taylor, M. J., and Kelley, M. C.: Two-dimensional spectral analysis of mesospheric airglow image data, Applied Optics., 36, 7374, https://doi.org/10.1364/AO.36.007374, 1997.

Haerendel, G., Eccles, J. V., and Çakir, S.: Theory for modeling the equatorial evening ionosphere and the origin of the shear in the horizontal plasma flow, J. Geophys. Res., 97, 1209–1223, https://doi.org/10.1029/91JA02226, 1992.

Huang, C. S. , Beaujardiere, O. D. L. , Roddy, P. A. , Hunton, D. E. , Ballenthin, J. O. , and Hairston, M. R.: Long-lasting daytime equatorial plasma bubbles observed by the c/nofs satellite, J. Geophys. Res., 118, 2398-2408, https://doi.org/10.1002/jgra.50252, 2013.

Huang, C. S.: Effects of the postsunset vertical plasma drift on the generation of equatorial spread f, Progress in Earth and Planetary Science., 5, 3, https://doi.org/10.1186/s40645-017-0155-4, 2018.

Katamzi-Joseph, Z. T., Habarulema, J. B., and Hernández-Pajares, M.: Midlatitude postsunset plasma bubbles observed over Europe during intense storms in April 2000 and 2001, Space Weather., 15, 1177–1190, https://doi.org/10.1002/2017SW001674, 2017.

Kelley, M. C., Fejer, B. G., and Gonzales, C. A.: An explanation for anomalous equatorial ionospheric electric fields associated with a northward turning of the interplanetary magneticfield, Geophys. Res. Lett., 6, 301-304, https://doi.org/10.1029/GL006i004p00301, 1979.

Kelley, M. C., Labelle, J., Kudeki, E., Fejer, B. G., Basu, S., Baker, K. D., Hanuise, C., Argo, P., Woodman, R.F., Swartz, W. E., Farley, D., and Meriwether, J.: The Condor Equatorial Spread F Campaign: Overview and results of the large-scale measurements, J. Geophys. Res., 91, 5487–5503, https://doi.org/10.1029/JA091iA05p05487,1986.

Kelley, M. C.: The Earth's Ionosphere: Plasma Physics and Electrodynamics, San Diego, CA: Academic, 2009.

Kil, H., Kintner, P. M., De Paula, E. R., and Kantor, I. J.: Global positioning system

https://doi.org/10.5194/angeo-2019-122
Preprint. Discussion started: 26 August 2019

measurements of the ionospheric zonal apparent velocity at cachoeira paulista in brazil, J. Geophys. Res., 105, 5317-5327, https://doi.org/10.1029/1999JA000244, 2000.

Lühr H., Xiong, C., Park, J., and Rauberg, J.: Systematic study of intermediate scale structures of equatorial plasma irregularities in the ionosphere based on CHAMP observations, Front Phys., 2, 15, https://doi.org/10.3389/fphy.2014.00015, 2014.

Makela, J. J., Kelley, M. C., and Nicolls, M. J.: Optical observations of the development of secondary instabilities on the eastern wall of an equatorial plasma bubble, J. Geophys. Res., 111, https://doi.org/ 10.1029/2006JA011646, 2006.

Makela, J. J., and Otsuka, Y.: Overview of Nighttime Ionospheric Instabilities at Low- and Mid-Latitudes: Coupling Aspects Resulting in Structuring at the Mesoscale, Space Science Reviews., 168, 419, https://doi.org/10.1007/s11214-011-9816-6, 2012.

Martinis, C., Eccles, J. V., Baumgardner, J., Manzano, J., and Mendillo, M.: Latitude dependence of zonal plasma drifts obtained from dual ‐ site airglow observations, J. Geophys. Res., 108, https://doi.org/10.1029/2002JA009462, 2003.

Ott, E.: Theory of Rayleigh-Taylor bubbles in the equatorial ionosphere, J. Geophys. Res., 83, 2066, https://doi.org/10.1029/JA083ia05p02066, 1978.

Park, S. H., England, S. L., Immel, T. J., Frey, H. U., and Mende, S. B.: A method for determining the drift velocity of plasma depletions in the equatorial ionosphere using far ‐ ultraviolet spacecraft observations, J. Geophys. Res., 112, A11, https://doi.org/10.1029/2007/JA012327, 2007.

Pimenta, A. A., Fagundes, P. R., Bittencourt, J. A., Sahai, Y., Gobbi, D., Medeiros, A. F., Taylor, M. J., and Takahashi, H.: Ionospheric plasma bubble zonal drift: a methodology using oi 630 nm all-sky imaging systems, Advances in Space Research., 27, 1219-1224, https://doi.org/10.1016/s0273-1177(01)00201-0, 2001.

Patra, A. K., Chaitanya, P. P., Dashora, N., Sivakandan, M., and Taori, A.: Highly localized unique electrodynamics and plasma irregularities linked with the 17 march 2015 severe magnetic storm observed using multitechnique common ‐

volume observations from gadanki, india, J. Geophys. Res., 121,518-11,527, https://doi.org/10.1002/2016JA023384, 2016.

Sahai, Y., Becker-Guedes, F., Fagundes, P. R., de Jesus, R., de Abreu, A. J., Otsuka, Y., Shiokawa, k., Igarashi, K., Yumoto, K., Huang, C. S., Lan, H. T., Saito, A., Guarnieri, F. L., Pillat, V. G., and Bittencourt, J. A.: Effects observed in the ionospheric F region in the east Asian sector during the intense geomagnetic disturbances in the early part of November 2004, J. Geophys. Res., 114, A00A18, https://doi.org/10.1029/2008JA013053, 2009.

Santos, A. M., Abdu, M. A., Souza, J. R., Sobral, J. H. A., Batista, I. S., and Denardini, C. M.: Storm time equatorial plasma bubble zonal drift reversal due to disturbance Hall electric field over the Brazilian region, J. Geophys. Res., 121, 5594–5612, https://doi.org/10.1002/2015JA022179, 2016.

Sheehan, R. E., and Valladares, C. E.: Equatorial ionospheric zonal drift model and vertical drift statistics from UHF scintillation measurements in South America, Ann. Geophys., 22, 3177–3193, https://doi.org/10.5194/angeo-22-3177-2004, 2004.

Scherliess, L., and Fejer, B. G.: Storm time dependence of equatorial disturbance dynamo zonal electric fields, J. Geophys. Res., 102, 24037–24046, https://doi.org/10.1029/97ja02165, 1997.

Taylor, M. J., Eccles, J. V., Labelle, J., and Sobral, J. H. A.: High resolution oi (630 nm) image measurements of f - region depletion drifts during the guará campaign, Geophys. Res. Lett., 24, 1699-1702, https://doi.org/10.1029/97g101207, 2013.

Tulasi, R. S., Rama, R. P. V. S., Prasad, D. S. V. V. D., Niranjan, K., Gopi, K. S., and Sridharan, R.: Local time dependent response of postsunset esf during geomagnetic storms, J. Geophys. Res., 113, A07310, https://doi.org/10.1029/2007/JA012922, 2008.

Weber, E., Buchau, J., and Moore, J.: Airborne studies of equatorial F layer ionospheric irregularities, J. Geophys. Res., 85, 4631–4641, https://doi.org/10.1029/JA0

85iA09p04631, 1980.

Xiong, C., Park, J., Lühr, H., Stolle, C., and Ma, S.Y.: Comparing plasma bubble occurrence rates at CHAMP and GRACE altitudes during high and low solar activity, Ann. Geophys., 28, 1647-1658, https://doi.org/10.5194/angeo-28-1647-2010, 2010.

Xiong, C., Lühr, H., and Fejer, B. G.: Global features of the disturbance winds during storm time deduced from CHAMP observations, J. Geophys. Res., 120, 5137–5150, https://doi.org/10.1002/2015JA021302, 2015.

Xiong, C., Stolle, C., Lühr, H., Park, J., Fejer, B. G., and Kervalishvili, G. N.: Scale analysis of the equatorial plasma irregularities derived from Swarm constellation, Earth Planets Space., 68, 121, https://doi.org/10.1186/s40623-016-0502-5, 2016.

Xiong, C., Xu, J., Wu, K., and Yuan, W.: Longitudinal thin structure of equatorial plasma depletions coincidently observed by swarm constellation and all-sky imager, J. Geophys. Res., 123, 3, https://doi.org/10.1002/2017JA025091, 2018.

Wu, K., Xu, J., Wang, W., Sun, L., Liu, X., and Yuan, W.: Interesting equatorial plasma bubbles observed by all-sky imagers in the equatorial region of China, J. Geophys. Res., 122, https://doi.org/10.1002/2017JA024561, 2017.

Wu, K., Xu, J., Xiong, C., and Yuan, W.: Edge plasma enhancements of equatorial plasma depletions observed by all-sky imager and the C/NOFS satellite, J. Geophys. Res., 123, 8835-8849, https://doi.org/10.1029/2018JA025809, 2018.

Yang, Z., Song, S., Jiao, W., Chen, G., and Xue, J.: Ionospheric tomography based on gnss observations of the cmonoc: performance in the topside ionosphere, GPS Solutions., 21, 363-375, https://doi.org/10.1007/s10291-016-0526-0, 2016.

Zhang, R., Liu, L., Chen, Y., and Le, H.: The dawn enhancement of the equatorial ionospheric vertical plasma drift, J. Geophys. Res., 120, 10,688-697, https://doi.org/10.1002/ 2015JA021972, 2015.

Zhang, R., Liu, L., Le, H., and Chen, Y.: Evidence and effects of the sunrise enhancement of the equatorial vertical plasma drift in the F region ionosphere, J. Geophys. Res., 121, 4826–4834, https://doi.org/10.1002/2016JA022491, 2016.

Zheng, J. , Zhao, B. , Xiong, B. , and Wan, W.: Spatial and temporal analysis of the total electron content over china during 2011–2014, Advances in Space Research., 57, 12, https://doi.org/10.1016/j.asr.2016.03.037, 2016.

Zhou, Y. L., Lühr, Hermann, Xiong, C., and Pfaff, R. F.: Ionospheric storm effects and equatorial plasma irregularities during the 17-18 march 2015 event, J. Geophys. Res., 121, 9146-9163, https://doi.org/10.1002/2016JA023122, 2016.

https://doi.org/10.5194/angeo-2019-122
Preprint. Discussion started: 26 August 2019

Figure Captions

Figure 1. The location of observation instruments. The red star denotes the geographic location of the all-sky imager at Qujing (25° N, 104° E). The blue circle denotes the field of view of the all-sky imager at an altitude of 250 km. The green dot denotes the geographic location of the digisond at Fuke (19.5° N, 109.1° E). The red dotted line represents the magnetic equator.

Figure 2. (a) *Kp* indexes, (b) the interplanetary magnetic field (IMF) *Bz*, (c) SYM/H, and (d) AE, AU, AL during 06-08 November 2015. (e) The variations of h'F obtained from the digisond at Fuke on 06-08 November 2015.

Figure 3. Images of equatorial plasma bubbles from the Qujing site between 05:15 LT and 06:21 LT on 08 November 2015. The observed images were mapped into geographical coordinates by assuming that the airglow emission layer was at an altitude of ~250 km. The white vertical line is a reference line of 106° E and horizontal line is a reference line of 25° N.

Figure 4. Total electron content residuals over China and adjacent areas with 10 minute interval during 04:30 – 08:20 LT on 08 November 2015. The black horizontal line is a reference line of 25° N.

Figure 5. Total electron content residuals correspond to each image of Figure 3. The black horizontal line is a reference line of 25° N. The black vertical line is a reference line of 106° E.

Figure 6. (a) N-S cross sections (between 104°E and 105°E) of the airglow images on 08 November 2015. (c) W-E cross sections (between 21.5°N and 22°N) of the airglow images. (e) W-E cross sections (between 18.5°N and 19°N) of the airglow images. (b) The variations of the meridian velocities of "b1" with local time. (d) and (f) The

variations of the zonal velocities of "b1" at ~ 22°N and ~19°N geographical latitudes, respectively.

Figure 7. Contours of nighttime zonal winds at 250 km in a range from 0° to 40° N in latitude and from 90° to 120° E in longitude during 08 November 2015. The dashed rectangles represent the location of EPBs.

Figure 8. The ionograms observed by the digisonde at Fuke between 04:00 LT and 07:30 LT on 08 November 2015.

Figure 9. The height of hmF2 in a range from 0° to 40° N in latitude and from 90° to 120° E in longitude during 08 November 2015. The red star represent the location of all-sky imager. The dashed rectangles represent the region of southeastern Qujing.

https://doi.org/10.5194/angeo-2019-122
Preprint. Discussion started: 26 August 2019

Annales Geophysicae
Discussions

Figure 1

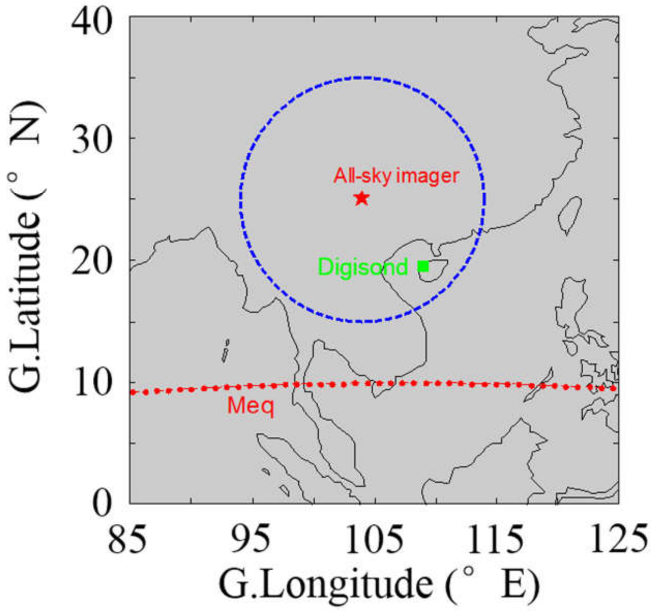

https://doi.org/10.5194/angeo-2019-122
Preprint. Discussion started: 26 August 2019

Annales Geophysicae
Discussions
Open Access
EGU

Figure 2

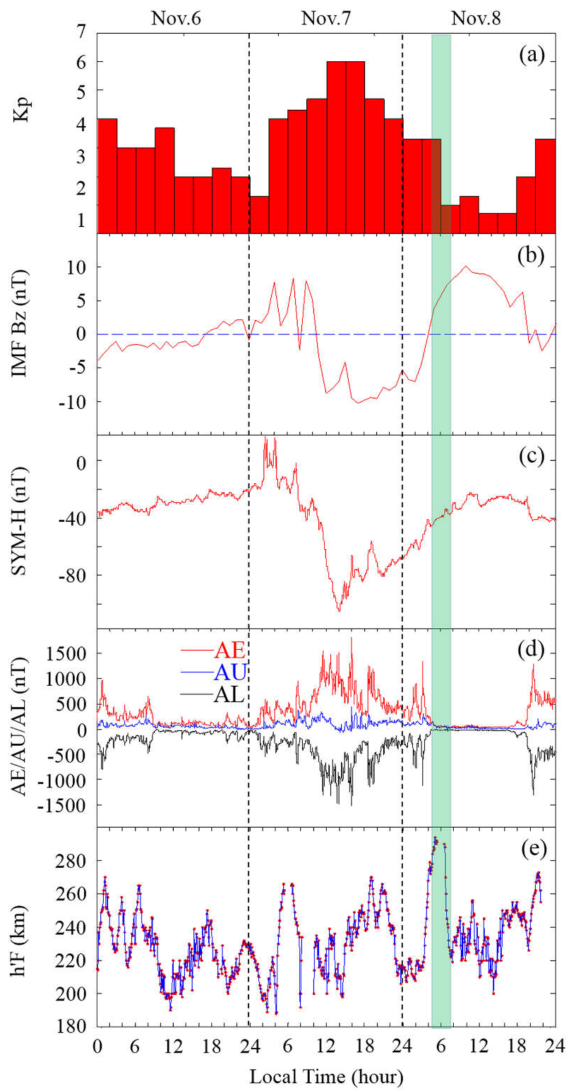

https://doi.org/10.5194/angeo-2019-122
Preprint. Discussion started: 26 August 2019

Annales Geophysicae Discussions Open Access EGU

Figure 3

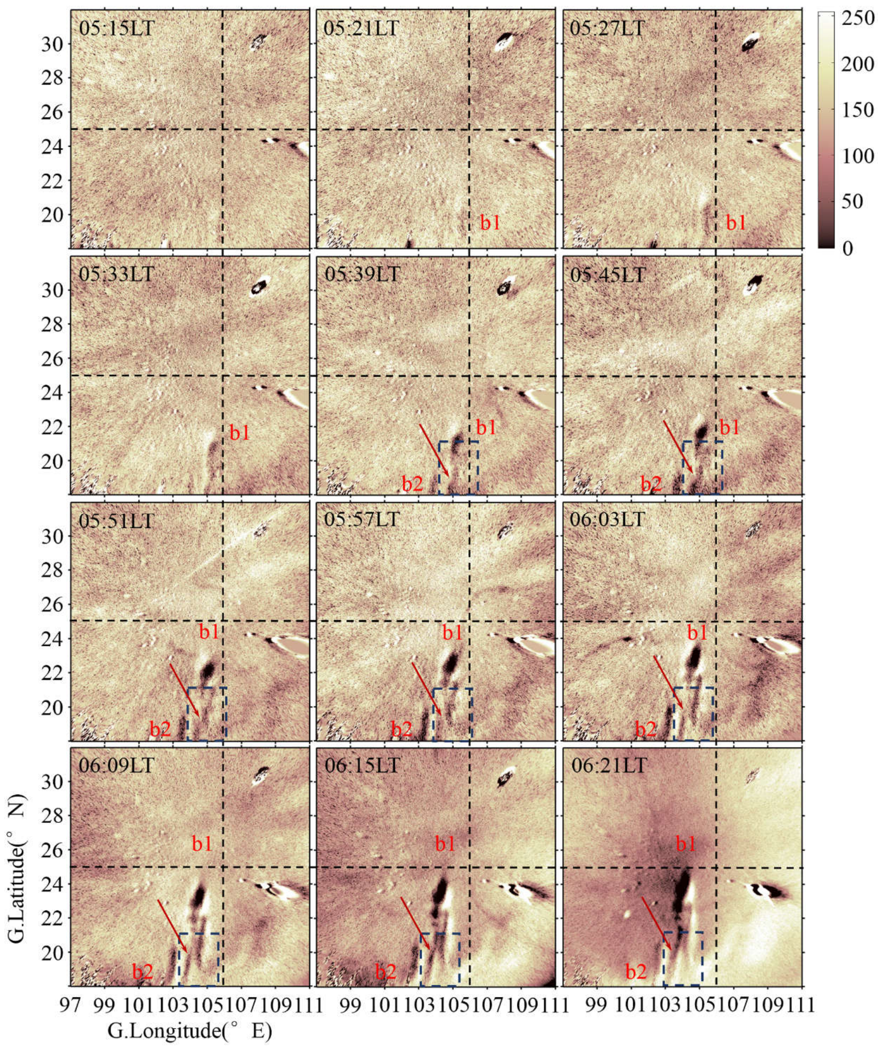

https://doi.org/10.5194/angeo-2019-122
Preprint. Discussion started: 26 August 2019

Figure 4

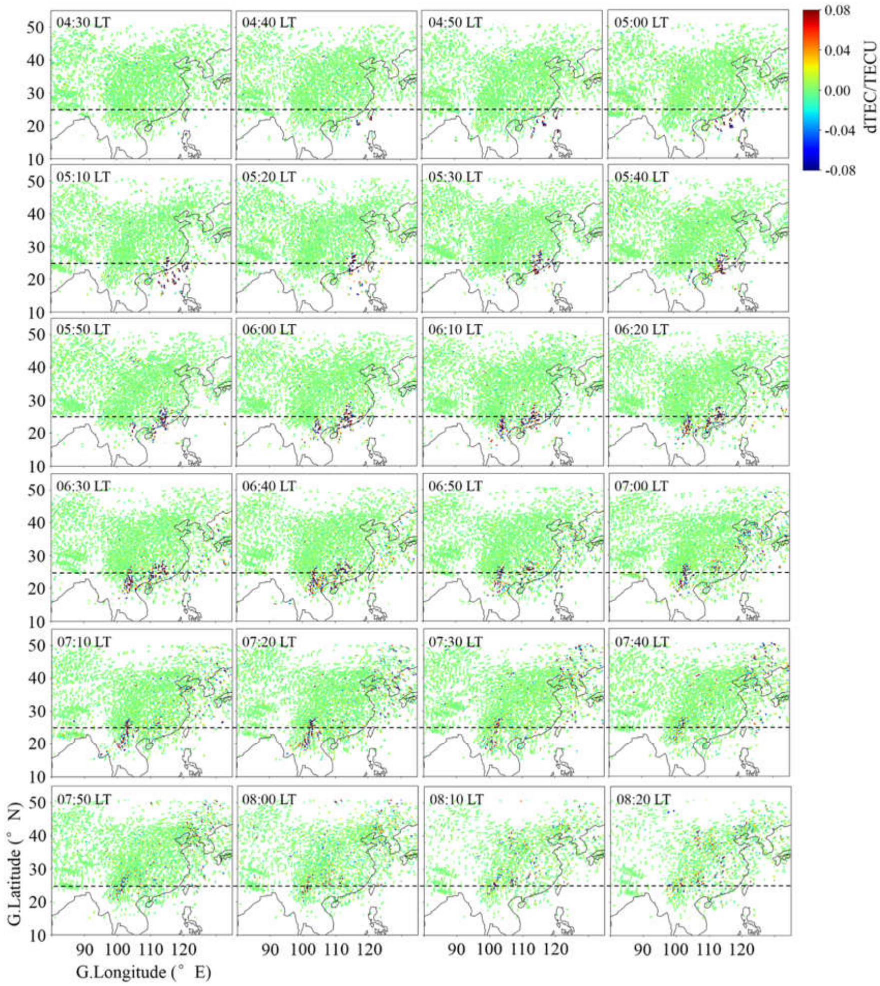

https://doi.org/10.5194/angeo-2019-122
Preprint. Discussion started: 26 August 2019

Figure 5

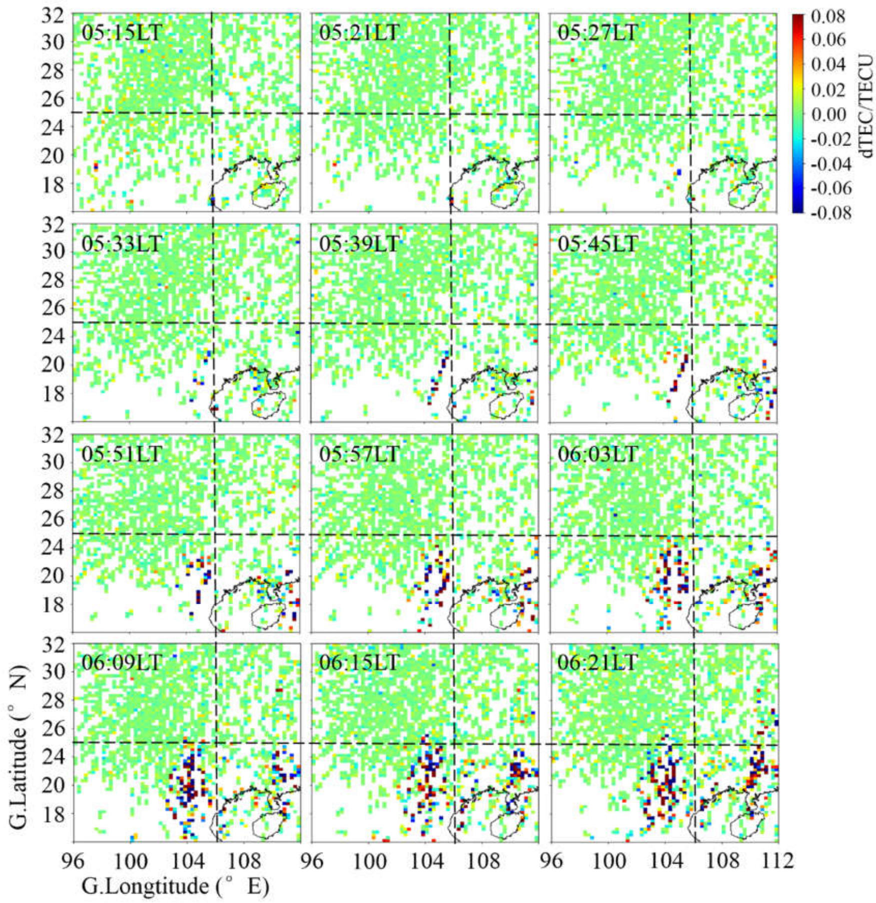

https://doi.org/10.5194/angeo-2019-122
Preprint. Discussion started: 26 August 2019

Annales Geophysicae Discussions

Figure 6

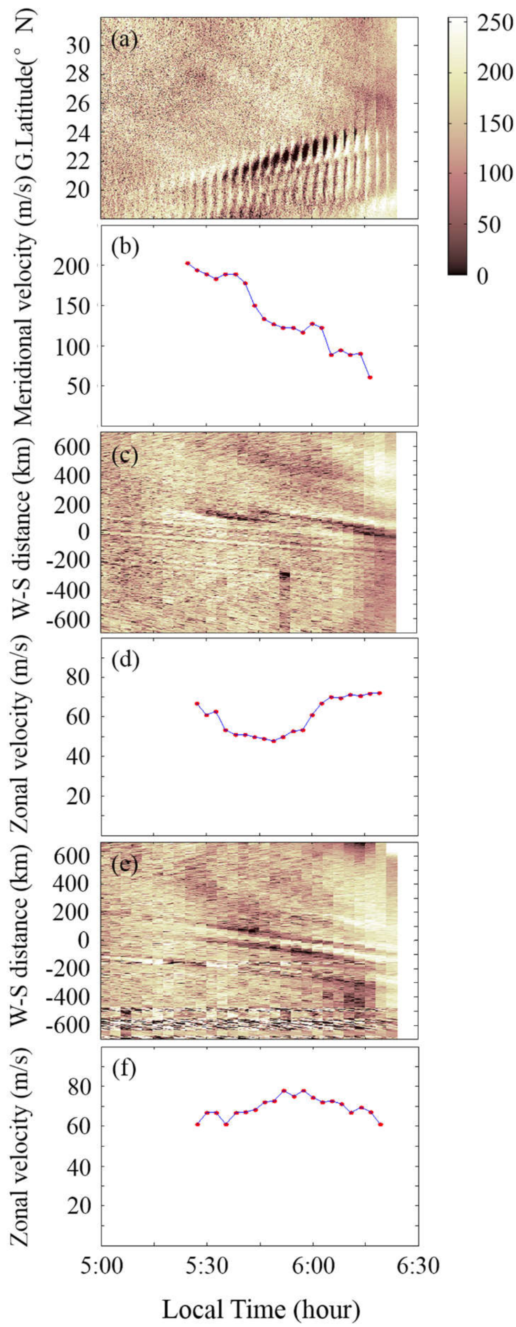

https://doi.org/10.5194/angeo-2019-122
Preprint. Discussion started: 26 August 2019

Figure 7

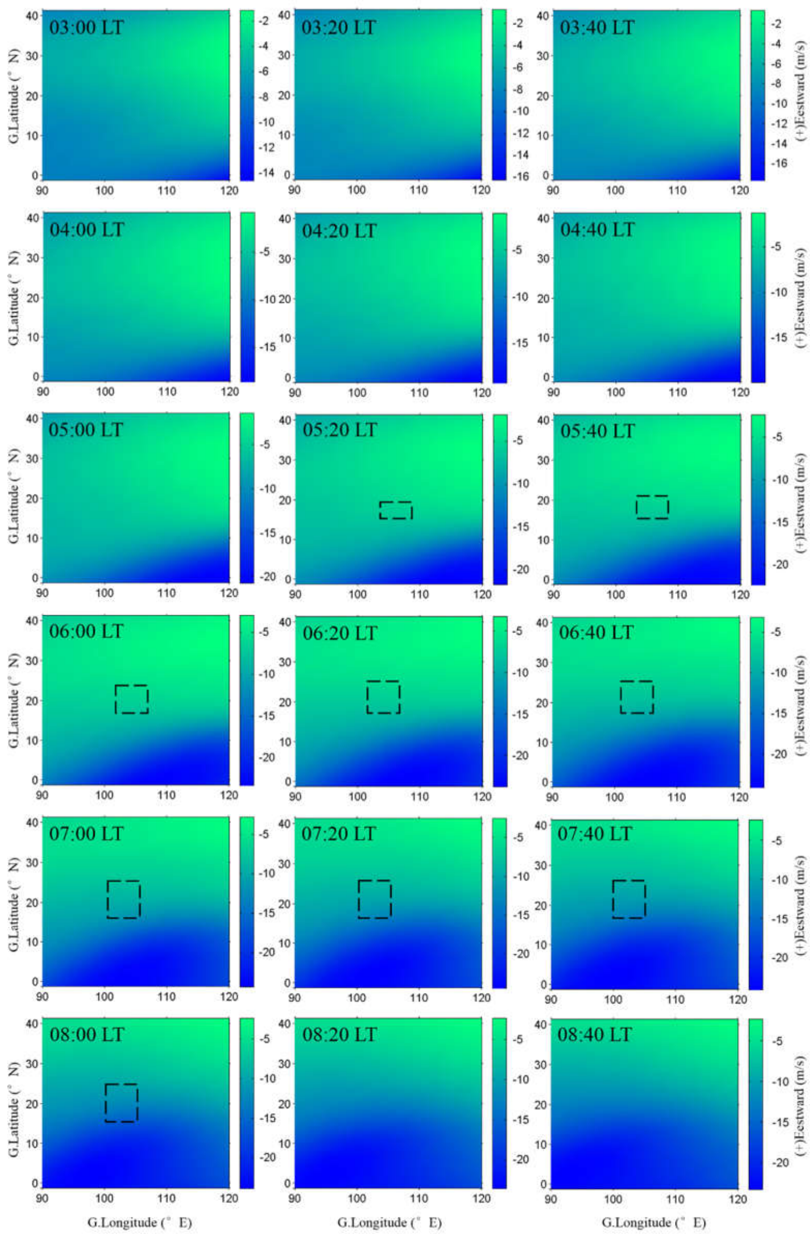

https://doi.org/10.5194/angeo-2019-122
Preprint. Discussion started: 26 August 2019

Figure 8

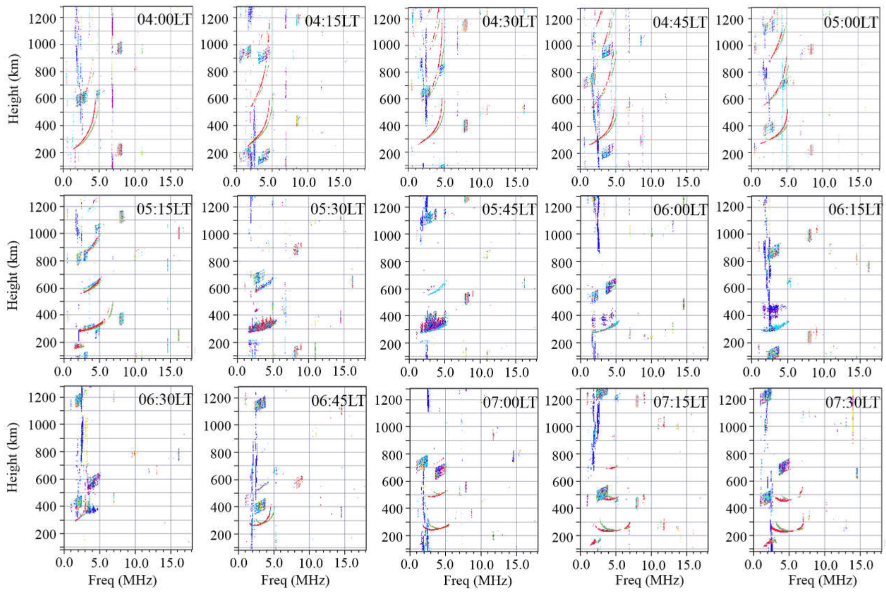

https://doi.org/10.5194/angeo-2019-122
Preprint. Discussion started: 26 August 2019

Annales Geophysicae
Discussions

Figure 9